Article

The Reaction of Tetrakis(dimethylamido)titanium with Self-Assembled Alkyltrichlorosilane Monolayers Possessing –OH, –NH, and –CH Terminal Groups

Aravind S. Killampalli, Paul F. Ma, and James R. Engstrom

J. Am. Chem. Soc., **2005**, 127 (17), 6300-6310• DOI: 10.1021/ja047922c • Publication Date (Web): 06 April 2005

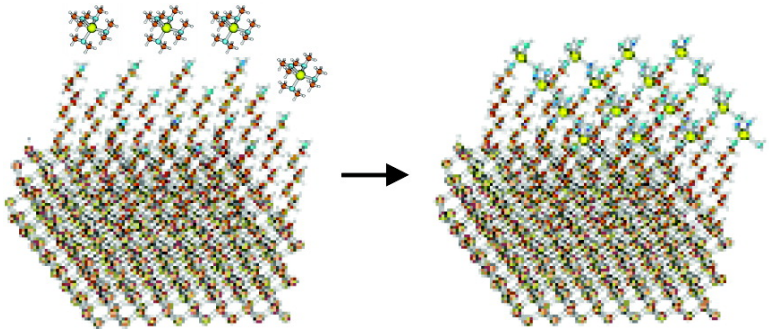

J|A|C|S
ARTICLES
Published on Web 04/06/2005

The Reaction of Tetrakis(dimethylamido)titanium with Self-Assembled Alkyltrichlorosilane Monolayers Possessing $-OH$, $-NH_2$, and $-CH_3$ Terminal Groups

Aravind S. Killampalli, Paul F. Ma, and James R. Engstrom*

Contribution from the School of Chemical and Biomolecular Engineering, Cornell University, Ithaca, New York 14853

Received April 10, 2004; E-mail: jre7@cornell.edu

Abstract: The reactions of tetrakis(dimethylamido)titanium, $Ti[N(CH_3)_2]_4$, with alkyltrichlorosilane self-assembled monolayers (SAMs) terminated by $-OH$, $-NH_2$, and $-CH_3$ groups have been investigated with X-ray photoelectron spectroscopy (XPS). For comparison, a chemically oxidized Si surface, which serves as the starting point for formation of the SAMs, has also been investigated. In this work, we examined the kinetics of adsorption, the spatial extent, and stoichiometry of the reaction. Chemically oxidized Si has been found to be the most reactive surface examined here, followed by the $-OH$, $-NH_2$, and $-CH_3$ terminated SAMs, in that order. On all surfaces, the reaction of $Ti[N(CH_3)_2]_4$ was relatively facile, as evidenced by a rather weak dependence of the initial reaction probability on substrate temperature ($T_s = -50$ to 110 °C), and adsorption could be described by first-order Langmuirian kinetics. The use of angle-resolved XPS demonstrated clearly that the anomalous reactivity of the $-CH_3$ terminated SAM could be attributed to reaction of $Ti[N(CH_3)_2]_4$ at the SAM/SiO_2 interface. Reaction on the $-NH_2$ terminated SAM proved to be the "cleanest", where essentially all of the reactivity could be associated with the terminal amine group. In this case, we found that approximately one $Ti[N(CH_3)_2]_4$ adsorbed per two SAM molecules. On all surfaces, there was significant loss of the $N(CH_3)_2$ ligand, particularly at high substrate temperatures, $T_s = 110$ °C. These results show for the first time that it is possible to attach a transition metal coordination complex from the vapor phase to a surface with an appropriately functionalized self-assembled monolayer.

I. Introduction

Inorganic−organic interfaces, owing to their unique chemical and electronic properties, are playing an increasingly important role in several technologies, including organic light-emitting diodes (OLEDs),[1,2] molecular electronics,[3−6] and microelectronic interconnect technology, for example, interfaces between carbon-based low-κ dielectrics and metallic/inorganic diffusion barriers.[7−9] Despite their importance, formation of these interfaces is not fully understood. Self-assembly is a popular method for making highly ordered (over nanometer length scales) organic monolayer films on metallic and semiconductor substrates.[10−12] These self-assembled "organic-on-inorganic" monolayers (SAMs) have been widely studied as model surfaces owing to their ease of formation, self-limiting growth characteristics, and the specificity of their reaction enabling the tailoring of surface properties by varying the functional end group. "Inorganic-on-organic" interfaces are also important in applications such as barrier layers (e.g., encapsulation of the aforementioned metallic interconnects), reflective coatings, and electrical contacts for both OLEDs and molecular electronics. Formation of these interfaces, however, is much less mature in comparison to formation of organic-on-inorganic interfaces constructed using SAMs. To date, the inorganic component of the interface has been a metal or an oxide formed by (elemental) evaporation in vacuum or by deposition in the liquid phase using a metal complex.

Formation of thin films on SAMs by liquid phase deposition has attracted recent interest. The reactions of $TiCl_4$,[13,15,17] $Ti(OCH(CH_3)_2)_4$,[14] aqueous titanium peroxide solutions,[16] $Ti(OC_2H_5)_2Cl_2$,[17] and $Ti(OC_2H_5)_4$[17] with alkyltrichlorosilane SAMs

(1) *Conjugated Polymer Surfaces and Interfaces, Electronic and Chemical Structure of Interfaces for Polymer Light Emitting Devices*; Salaneck, W. R., Stafstrom, S., Bredas, J.-L., Eds.; Cambridge University Press: Cambridge, 1996.
(2) Yan, L.; Gao, Y. *Thin Solid Films* **2002**, *417*, 101−106.
(3) *Molecular Electronics: Science and Technology*; Aviram, A., Ratner, M., Eds.; NY Academy of Science: New York, 1998; Vol. 852.
(4) Ishii, H.; Sugiyama, K.; Ito, E.; Seki, K. *Adv. Mater.* **1999**, *11*, 605−625.
(5) Chen, J.; Reed, M. A.; Dirk, S. M.; Price, D. W.; Rawlett, A. M.; Tour, J. M.; Grubisha, D. S.; Bennett, D. W. *NATO Sci. Ser. II: Math., Phys. Chem.* **2003**, *96*, 59−195.
(6) Haynie, B. C.; Walker, A. V.; Tighe, T. B.; Allara, D. L.; Winograd, N. *Appl. Surf. Sci.* **2003**, *203*−*204*, 433−436.
(7) Hsu, Y.; Standaert, T. E. F. M.; Oehrlein, G. S.; Kuan, T. S.; Sayre, E.; Rose, K.; Lee, K. Y.; Rossnagel, S. M. *J. Vac. Sci. Technol. B* **1998**, *16*, 3344−3348.
(8) Rossnagel, S. M. *J. Vac. Sci. Technol. B* **2002**, *20*, 2328−2336.
(9) Elam, J. W.; Wilson, C. A.; Schuisky, M.; Sechrist, Z. A.; George, S. M. *J. Vac. Sci. Technol. B* **2003**, *21*, 1099−1107.
(10) *An Introduction to Ultrathin Organic Films, From Langmuir*−*Blodgett to Self-Assembly*; Ulman, A., Ed.; Academic Press: Boston, MA, 1991.
(11) Dubois, L. H.; Nuzzo, R. G. *Annu. Rev. Phys. Chem.* **1992**, *43*, 437−463.
(12) Ulman, A. *Chem. Rev.* **1996**, *96*, 1533−1554.
(13) Shin, H.; Collins, R. J.; De Guire, M. R.; Heuer, A. H.; Sukenik, C. N. *J. Mater. Res.* **1995**, *10*, 692−698.
(14) Shin, H.; Collins, R. J.; De Guire, M. R.; Heuer, A. H.; Sukenik, C. N. *J. Mater. Res.* **1995**, *10*, 699−703.
(15) Xiao, Z.; Minhua, X.; Jianhua, G.; Dang, H.; Zuhong, L. *Mater. Chem. Phys.* **1998**, *52*, 170−174.
(16) Niesen, T. P.; Bill, J.; Aldinger, F. *Chem. Mater.* **2001**, *13*, 1552−1559.
(17) Masuda, Y.; Jinbo, Y.; Yonezawa, T.; Koumoto, K. *Chem. Mater.* **2002**, *14*, 1236−1241.

10.1021/ja047922c CCC: $30.25

bearing sulfonate,[13,15,16] hydroxyl,[14,16] amine,[16] and methyl[17] groups, phenyltrichlorosilane,[17] and (aminopropyl)triethoxysilane[17] SAMs have been investigated. X-ray photoelectron spectroscopy (XPS) has been used to probe elemental composition,[14−17] and film morphology[13] has been studied. Vapor phase evaporative deposition of elemental metals on functionalized SAMs has also been studied. Jung and Czanderna[18−20] examined the evaporation of elemental metals onto SAMs with different organic functional end groups (OFGs) and categorized metal/OFG interactions to be "strong" (e.g., Cr/COOH or Cu/COOH where metals react primarily with the OFG) or "weak" (e.g., Cu/OH, Cu/CN, Ag/CH_3, or Ag/COOH where metals penetrate the SAM). Using in situ XPS analysis, Allara and co-workers[21] found elemental titanium to be highly reactive with the $-OH$, $-CN$, and $-COOCH_3$ terminated alkanethiol SAMs, forming TiO_x and TiN_x species at low coverages and TiC_x species at high coverages, possibly due to reaction with the SAM backbone. Allara and co-workers[22,24] also studied the reaction of elemental aluminum with $-CH_3$, $-COOCH_3$, and $-COOH$[23] terminated alkanethiol self-assembled monolayers on polycrystalline gold. While significant penetration of Al to the SAM/Au interface was observed for the $-CH_3$ terminated SAM, reaction of Al with the $-COOCH_3$ and $-COOH$ terminated SAMs was confined to the SAM/vacuum interface. The deposition of thin inorganic films on SAMs using organometallic precursors has received relatively less attention despite the fact that such a process might provide superior control over interface formation. Of the few studies that have been conducted, spatial selectivity and thin film morphology were examined during the formation of Au and Pd films on thiol SAMs.[25] For Al deposition from trimethylamine alane on $-OH$, $-COOH$, and $-CH_3$ terminated thiol SAMs,[26,27] interfacial chemistry was examined using XPS, but an explicit examination of the kinetics of adsorption was not attempted. Among these studies, Woell et al.[26] carried out the sole study of interface formation in ultrahigh vacuum (UHV).

We present results here concerning the adsorption and reaction of a titanium coordination compound, tetrakis(dimethylamido)titanium ($Ti[N(CH_3)_2]_4$), with alkyltrichlorosilane SAMs terminated by $-OH$, $-NH_2$, and $-CH_3$ groups. The adsorption of $Ti[N(CH_3)_2]_4$ on functionalized SAMs was chosen as a model for the first key reaction to inorganic thin film deposition of titanium nitride (TiN) on organic surfaces. Bradley and co-workers[28,29] carried out early studies of the reactions of $Ti[N(CH_3)_2]_4$ with NH_3 to form titanium nitride films in solution and reported facile transamination reactions leading to multiple metal−nitrogen bonds. More recently, TiN films have been employed as diffusion barriers in microelectronic circuits owing to their excellent chemical and thermal stability, low bulk resistivity, and excellent adhesion.[30−34] Although $TiCl_4$ has been used as a precursor for TiN films, the temperatures involved are too high for microelectronic processing and Cl contamination is a significant problem.[35,36] Consequently, other precursors have been explored, and $Ti[N(CH_3)_2]_4$, in particular, has been studied extensively as a precursor for the formation of TiN thin films via chemical vapor (CVD)[37−51] and atomic layer deposition (ALD)[52−55] techniques. In this study, we employ X-ray photoelectron spectroscopy to quantify the kinetics of adsorption of the titanium precursor, $Ti[N(CH_3)_2]_4$, and as a tool to probe the spatial extent of reaction (e.g., surface vs subsurface adsorption). As such, this represents the first in depth study, carried out in UHV, of the reaction of a transition metal complex with a set of SAMs possessing different functional end groups.

II. Experimental Procedures

All experiments involved three sequential stages. First, trichlorosilane SAMs were formed on SiO_2 surfaces. In some cases, following SAM formation, the substrates were subjected to additional chemical conversion steps to form the desired organic functional end group. Second,

(18) Jung, D. R.; Czanderna, A. W. *Crit. Rev. Solid State Mater. Sci.* **1994**, *19*, 1−54.
(19) Herdt, G. C.; Jung, D. R.; Czanderna, A. W. *Prog. Surf. Sci.* **1995**, *50*, 103−129.
(20) Jung, D. R.; Czanderna, A. W.; Herdt, G. C. *J. Vac. Sci. Technol. A* **1996**, *14*, 1779−1787.
(21) Konstadinidis, K.; Zhang, P.; Opila, R. L.; Allara, D. L. *Surf. Sci.* **1995**, *338*, 300−312.
(22) Fisher, G. L.; Hooper, A.; Opila, R. L.; Jung, D. R.; Allara, D. L.; Winograd, N. *J. Electron. Spectrosc. Relat. Phenom.* **1999**, *98*−*99*, 139−148.
(23) Fisher, G. L.; Hooper, A. E.; Opila, R. L.; Allara, D. L.; Winograd, N. *J. Phys. Chem. B* **2000**, *104*, 3267−3273.
(24) Hooper, A.; Fisher, G. L.; Konstadinidis, K.; Jung, D.; Nguyen, H.; Opila, R.; Collins, R. W.; Winograd, N.; Allara, D. L. *J. Am. Chem. Soc.* **1999**, *121*, 8052−8064.
(25) Fischer, R. A.; Weckenmann, U.; Winter, C.; Kashammer, J.; Scheumann, V.; Mittler, S. *J. Phys. IV: Proc.* **2001**, *11*, Pr3/1183−Pr3/1190.
(26) Weiss J.; Himmel, H. J.; Fischer, R. A.; Woell, C. *Chem. Vap. Deposition* **1998**, *4*, 17−21.
(27) Wohlfart, P.; Weiss, J.; Kashammer, J.; Kreiter, M.; Winter, C.; Fischer, R.; Mittler-Neher, S. *Chem. Vap. Deposition* **1999**, *5*, 165.
(28) Bradley, D. C.; Thomas, I. M. *J. Chem. Soc.* **1960**, 3857−3861.
(29) Bradley, D. C.; Torrible, E. G. *Can. J. Chem.* **1963**, *41*, 134−138.
(30) Kaloyeros, A. E.; Eisenbraun, E. *Annu. Rev. Mater. Sci.* **2000**, *30*, 363−385.
(31) (a) Eizenberg, M. *MRS Bull.* **1995**, *20*, 38−41. (b) *Some Fundamental Issues on Metallization in VLSI*; Ferry, D. K., Kozicki, M. N., Raupp, G. B., Eds.; SPIE: San Jose, CA, 1991.
(32) Wang, S.-Q.; Raaijmakers, I.; Burrow, B. J.; Suthar, S.; Redkar, S.; Kim, K.-B. *J. Appl. Phys.* **1990**, *68*, 5176−5187.
(33) Moriyama, M.; Kawazoe, T.; Tanaka, M.; Murakami, M. *Thin Solid Films* **2002**, *416*, 136−144.
(34) Okada, L. A.; George, S. M. *Appl. Surf. Sci.* **1999**, *137*, 113−124.
(35) (a) Kurtz, S. R.; Gordon, R. G. *Thin Solid Films* **1986**, *140*, 277−290. (b) Ritala, M.; Leskela, M.; Rauhala, E.; Haussalo, P. *J. Electrochem. Soc.* **1995**, *142*, 2731−2737. (c) Ritala, M.; Asikainen, T.; Leskela, M.; Jokinen, J.; Lappalainen, R.; Utriainen, M.; Niinisto, L.; Ristolainen, E. *Appl. Surf. Sci.* **1997**, *120*, 199−212. (d) Uhm, J.; Jeon, H. *Jpn. J. Appl. Phys.* **2001**, *40*, 4657−4660.
(36) Yokoyama, N.; Hinode, K.; Homma, Y. *J. Electrochem. Soc.* **1991**, *138*, 190−195.
(37) Sugiyama, K.; Pac, S.; Takahashi, Y.; Motojima, S. *J. Electrochem. Soc.* **1975**, *122*, 1545−1549.
(38) Ishihara, K.; Yamakazi, K.; Hamada, H.; Kamisako, K.; Tarui, Y. *Jpn. J. Appl. Phys.* **1990**, *29*, 2103−2105.
(39) (a) Fix, R. M.; Gordon, R. G.; Hoffman, D. M. *Mater. Res. Soc. Symp. Proc.* **1990**, *168*, 357−362. (b) Fix, R. M.; Gordon, R. G.; Hoffman, D. M. *Chem. Mater.* **1990**, *2*, 235−241.
(40) (a) Fix, R. M.; Gordon, R. G.; Hoffman, D. M. *J. Am. Chem. Soc.* **1990**, *112*, 7833−7835. (b) Fix, R. M.; Gordon, R. G.; Hoffman, D. M. *Chem. Mater.* **1991**, *3*, 1138−1148.
(41) Raaijmakers, I. J.; Vrtis, R. N.; Yang, J.; Ramaswami, S.; Lagendijk, A.; Roberts, D. A.; Broadbent, E. K. *Mater. Res. Soc. Symp. Proc.* **1992**, *260*, 99−105.
(42) Katz, A.; Feingold, A.; Nakahara, S.; Pearton, S. J.; Lane, E.; Geva, M.; Stevie, F. A.; Jones, K. *Jpn. J. Appl. Phys.* **1992**, *71*, 993−1000.
(43) Dubois, L. H.; Zegarski, B. R.; Girolami, G. S. *J. Electrochem Soc.* **1992**, *139*, 3603−3609.
(44) (a) Prybyla, J. A.; Chiang, C.-M.; Dubois, L. H. *J. Electrochem. Soc.* **1993**, *140*, 2695−2702. (b) Dubois, L. H. *Polyhedron* **1994**, *13*, 1329−1336.
(45) Truong, C. M.; Chen, P. J.; Corneille, J. S.; Oh, W. S.; Goodman, D. W. *J. Phys. Chem.* **1995**, *99*, 8831−8842.
(46) Gordon, R. G.; Musher, J. N. *J. Mater. Res.* **1996**, *11*, 989−1001.
(47) Weiller, B. H. *J. Am. Chem. Soc.* **1996**, *118*, 4975−4983.
(48) Ruhl, G.; Rehmet, R.; Knizova, M.; Merica, R.; Vepřek, S. *Chem. Mater.* **1996**, *8*, 2712−2720.
(49) Cundari, T. R.; Morse, J. M., Jr. *Chem. Mater.* **1996**, *8*, 189−196.
(50) Driessen, J. P. A. M.; Schoonman, J.; Jensen, K. F. *J. Electrochem. Soc.* **2001**, *148*, G178−G184.
(51) Amato-Wierda, C.; Norton, E. T., Jr. *Chem. Mater.* **2001**, *13*, 4655−4660.
(52) Lim, J.-W.; Park, H.-S.; Kang, S.-W. *J. Electrochem. Soc.* **2001**, *148*, C403−C408.
(53) Kim, H. K.; Kim, J. Y.; Park, J. N.; Kim, Y.; Kim, Y. D.; Jeon, H.; Kim, W. M. *J. Korean Phys. Soc.* **2002**, *41*, 739−744.
(54) Kim, J. Y.; Choi, G. H.; Kim, Y. D.; Kim, Y.; Jeon, H. *Jpn. J. Appl. Phys. Part 1* **2003**, *42*, 4245−4248.
(55) Elam, J. W.; Schuisky, M.; Ferguson, J. D.; George, S. M. *Thin Solid Films* **2003**, *436*, 145−156.

and prior to insertion into vacuum, the substrates were characterized using contact angle measurements, ellipsometry, and atomic force microscopy (AFM). Third, the substrates were transferred into a custom-designed UHV chamber[56] for additional analysis using XPS and eventual exposure to the titanium coordination complex. Once in the UHV chamber, XPS was used to determine the coverage−exposure relationship for $Ti[N(CH_3)_2]_4$ on the different SAMs, and in selected cases, angle-resolved XPS (ARXPS) was used to probe the spatial extent of reaction of the precursor.

A. Formation of the Self-Assembled Monolayers. Materials. The following chemicals were used as received: hexadecane, chloroform, and carbon tetrachloride, all anhydrous and >99%; tetrahydrofuran (THF), >99%, A.C.S. reagent; 1.0 M borane−tetrahydrofuran (BH_3−THF) complex; 37% hydrochloric acid, A.C.S. reagent; 30% hydrogen peroxide, A.C.S. reagent; sodium hydroxide pellets, reagent grade (all from Sigma-Aldrich Corp., St. Louis, MO); trichlorosilane precursors (Gelest Inc., Morrisville, PA), 11-cyanoundecyltrichlorosilane, 10-undecenyltrichlorosilane, and *n*-octadecyltrichlorosilane; $Ti[N(CH_3)_2]_4$ (Schumacher, Carlsbad, CA) ≥99.999% purity based on metals analyzed and ≥99% purity based on an assay by NMR; CMOS grade acetone, CMOS grade 2-propanol, and buffered oxide etch (BOE) (6:1 CMOS grade NH_4F−HF aqueous solution) (Mallinckrodt Baker Inc., Phillipsburg, NJ); Nanostrip (Cyantek Corp., Fremont, CA). The solvents, 99% dicyclohexyl, and THF (Fisher Scientific International Inc., Springfield, NJ) were dried using 8 mesh Drierite (W. A. Hammond Drierite Co. Ltd., Xenia, OH). Chloroform, 99.8% HPLC grade with 50 ppm pentene (Fisher Scientific), was used to sonicate freshly cleaved silicon wafers.

Substrate Preparation. The starting substrates were 100 mm single side polished, 500−550 μm thick Si (100) wafers, doped with boron (38−63 Ωcm), which were cut into squares (16.75 × 16.75 mm^2). Next, a layer of silicon dioxide 20−25 Å thick was grown (details in Supporting Information), which is fully wet by water with an advancing contact angle of 0° and a receding contact angle of 0°.[57] This oxide has been reported to possess ∼5 × 10^{14} SiOH groups/cm^2,[58,59] and is the "chemical oxide" referred to below.

SAM Formation. All SAMs were formed by liquid phase deposition on chemical oxide. Solvents used were 4:1 hexadecane/chloroform for octadecyltrichlorosilane ($Cl_3-Si-(CH_2)_{17}-CH_3$), and bicyclohexyl for 10-undecenyltrichlorosilane ($Cl_3-Si-(CH_2)_9-CH=CH_2$) and 11-cyanoundecyltrichlorosilane ($Cl_3-Si-(CH_2)_{11}-CN$). These solvents were chosen taking into account their freezing point and the transition temperature (10 °C for 11 carbon chains and 28 °C for 18 carbon chains) to be maintained for the formation of well-ordered SAMs.[60,61] All solutions were ∼2.5 mM concentration of the SAM precursor molecule in the solvent. Substrates were dipped in the SAM solution for 1 h (−CH=CH_2 and $-CH_3$ terminated SAM) or 3 min (−CN terminated SAM) and then sonicated in anhydrous chloroform for 10−25 min to remove polymerized residue not bonded to the substrate. Finally, the substrates were washed in DI water, dried with N_2, and stored in precleaned fluoroware containers in a desiccator.

Formation of Terminal Groups. The vinyl terminated SAM (≡Si−$(CH_2)_9$−CH=CH_2) was converted to an −OH terminated SAM by hydroboration (≡Si−$(CH_2)_9-CH_2-CH_2OH$). This treatment has been found to convert ∼97% of the vinyl groups to −OH groups for a 16 carbon SAM.[58] The −CN terminated SAM (≡Si−$(CH_2)_{11}$−CN) was converted into an $-NH_2$ terminated SAM, also by hydroboration (≡Si−$(CH_2)_{11}-CH_2-NH_2$). This treatment has been found to reduce the −CN group completely[62] (details in Supporting Information).

B. Characterization of the Self-Assembled Monolayers. Contact Angle Measurements. Contact angle measurements were carried out employing a NRL CA goniometer (Rame-Hart Inc., Mountain Lakes, NJ), with an advancing (receding) droplet volume of about 3 (2) μL. Contact angles were measured on each side of the droplet and in five different areas on each sample, and the average of these values is reported. Typical values for the standard deviation were 2−3°.

Ellipsometry. Measurements of the thickness of the SAMs were performed with a Gaertner L-120A ellipsometer (He−Ne 632.8 nm laser, incident at 70°). For the refractive indices, a value of 1.46 has been reported for the chemical oxide,[63] whereas values of 1.42−1.44 have been reported for the SAMs examined here, similar to straight-chain saturated hydrocarbons.[58] Sensitivity of the calculated thickness to the value assumed for the refractive index was small—a change of 0.05 resulted in less than a 1 Å change in the estimated thickness of the monolayer. Therefore, the thickness of the chemical oxide was subtracted from a measurement of the thickness of the combined chemical oxide/SAM layer, assuming a refractive index of 1.46 for the composite layer, to yield the thickness of the SAM. Measurements of this type were made in 3−5 different areas on each sample and repeated on different samples (estimated error is ±1 Å).

Atomic Force Microscopy (AFM). Images were acquired with a Dimension 3100 scanning probe microscope (Veeco Instruments, Woodbury, NY) in tapping mode using Tap 300 SPM probes (Nanodevices Inc., Santa Barbara, CA).

X-ray Photoelectron Spectroscopy (XPS). XPS was carried out using a VSW twin anode X-ray source (Mg/Al) and a VSW CLASS 100 concentric hemispherical energy analyzer (VSW Worldwide, Cheshire, U.K.). Mg Kα X-rays (1253.6 eV) were used throughout this study. Survey scans (e.g., 0−1300 eV kinetic energy) were carried out in the fixed retardation ratio mode, whereas detailed scans (range of ∼20 eV over a single feature) were carried out in the fixed analyzer transmission mode. Short scans (0.5 eV/s, 10 cycles) were used for C(1s), O(1s), Si(2p), Ti(2p), and N(1s) peaks. Consequently, damage to the SAMs due to exposure to the X-rays was not manifest in the experiments reported here.[64] The takeoff angle for photoelectrons was 38.5° with respect to the surface normal for experiments examining the kinetics of adsorption (analysis area 5 mm diameter) and 0−65° for ARXPS (analysis area 1 × 10 mm^2 rectangle). All experiments involving ARXPS were conducted at T_s = 110 °C. A background subtraction method first proposed by Shirley[65] was used in all analyses of the peaks. Peak areas and peak positions were obtained by fitting the spectra to a product Gaussian−Lorentzian (G−L) function with a mixing ratio of 0.9.[66,67]

C. Study of the Reaction of $Ti[N(CH_3)_2]_4$ with the SAMs. UHV Apparatus. Exposure of SAM surfaces to $Ti[N(CH_3)_2]_4$ was carried out in a custom-designed ultrahigh vacuum system described in detail elsewhere.[56] A microcapillary array doser (Burle Technologies Inc., Lancaster, PA) made of lead silicate glass was used to deliver a uniform flux of $Ti[N(CH_3)_2]_4$ to the surface of the sample. An estimate for the absolute throughput of $Ti[N(CH_3)_2]_4$ leaving the doser was made to be 4.171 × 10^{14} molecules/s (details in Supporting Information). Using established correlations for the angular distribution produced by capillary array dosers,[68] we computed the fraction of the flux that was intercepted by the sample. Accounting for the sample area and the angle

(56) Xia, L.-Q.; Jones, M. E.; Maity, N.; Engstrom, J. R. *J. Vac. Sci. Technol. A* **1995**, *13*, 2651−2664.
(57) Liebmann-Vinson, A.; Lander, L. M.; Foster, M. D.; Brittain, W. J.; Vogler, E. A.; Majkrzak, C. F.; Satija, S. *Langmuir* **1996**, *12*, 2256−2262.
(58) Wasserman, S. R.; Tao, Y.-T.; Whitesides, G. M. *Langmuir* **1989**, *5*, 1074−1087.
(59) Sung, M. M.; Kluth, G. J.; Maboudian, R. *J. Vac. Sci. Technol. A* **1999**, *17*, 540−544.
(60) Brzoska, J. B.; Azouz, I. B.; Rondelez, F. *Langmuir* **1994**, *10*, 4367−4373.
(61) Kluth, G. J.; Sung, M. M.; Maboudian, R. *Langmuir* **1997**, *13*, 3775−3780.
(62) Balachander, N.; Sukenik, C. N. *Langmuir* **1990**, *6*, 1621−1627.
(63) *Handbook of Optical Constants of Solids*; Palik, E. D., Ed.; Academic Press: New York, 1985.
(64) Frydman, E.; Cohen, H.; Maoz, R.; Sagiv, J. *Langmuir* **1997**, *13*, 5089−5106.
(65) Shirley, D. A. *Phys. Rev. B* **1972**, *5*, 4709−4714.
(66) *Practical Surface Analysis: Volume I, Auger and X-ray Photoelectron Spectroscopy*, 2nd ed.; Seah, M. P., Briggs, D., Eds.; John Wiley and Sons: Chichester, England, 1990.
(67) Conny, J. M.; Powell, C. J. *Surf. Interface Anal.* **2000**, *29*, 856−872.
(68) Campbell, C. T.; Valone, S. M. *J. Vac. Sci. Technol. A* **1985**, *3*, 408−411.

Table 1. Properties of Self-Assembled Monolayers[a]

surface	Contact Angle advancing	Contact Angle receding	Contact Angle hysteresis	thickness (ellipsometry)	density (cm^{-2}, XPS)	roughness (AFM)
chemical oxide	<15°	<10°		20−25 Å		3.02 Å
≡Si−(CH$_2$)$_{17}$−CH$_3$	112 ± 0.6°	109.7 ± 4.7°	2.3°	27 Å	3.09 × 10^{14} 3.99 × 10^{14}	4.19 Å
	110−112° [b]			27.5 Å[c]		
≡Si−(CH$_2$)$_{10}$−CH$_2$OH	54.9 ± 1.7°	50.4 ± 2.2°	4.5°	17 Å	2.96 ×10^{14}	4.04 Å
	50−60° [c]			16 Å[c]		
≡Si−(CH$_2$)$_{12}$−NH$_2$	59.4 ± 3.9°	47.0 ± 3.4°	12.4°		4.38 × 10^{14}	4.44 Å
	63 ± 2.0° [d]	42.0 ± 4.0° [d]	21.0° [d]			

[a] This work unless otherwise indicated. [b] From ref 10. [c] From ref 36. [d] From ref 40.

of incidence, θ_i, gives the incident flux of Ti[N(CH$_3$)$_2$]$_4$ (2.80 × 10^{13} molecules/cm^2/s). We estimate that the variation of the flux over the area sampled by XPS is no greater than ±1.5%, whereas the absolute accuracy is ca. ±30%.

Experimental Procedures. All SAM films were deposited on chemical oxide, as described above. A polycrystalline Au sample (e-beam evaporated 1000 Å of Au, and 100 Å of Cr, on a Si(100) wafer with a native oxide layer) was used as reference standard for XPS. After acquiring an XP spectrum of the Au(4f) peak, the SAM-coated substrate was transferred into the UHV chamber via a fast-entry load-lock. Once a base pressure of ca. 2 × 10^{-9} Torr was achieved, experiments involving Ti[N(CH$_3$)$_2$]$_4$ were initiated. First, the sample was brought to temperature (here, either −50, 30, or 110 °C). These temperatures are below those (125 and 140 °C) that have been reported to lead to SAM degradation upon annealing at much higher pressures (10^{-2}−10^{-3} Torr) and for long periods of time.[69] Second, XP spectra were obtained (vide supra) to verify SAM identity and to quantify the coverage. Next, the SAM surface was exposed to Ti[N(CH$_3$)$_2$]$_4$ through the doser, where exposures ranged from 45 to 390 s. After each exposure, the Ti(2p) peak was scanned (vide infra) in order to quantify Ti[N(CH$_3$)$_2$]$_4$ adsorption on the SAM surface. These steps were repeated until saturation of the adlayer was apparent. After the final exposure, detailed scans of C(1s), O(1s), N(1s), and Si(2p) peaks were obtained.

III. Results and Discussion

A. Characterization of the Self-Assembled Monolayers: The Reactive Surface. The chemical oxide and the three SAM surfaces were characterized by measurements of the contact angle, ellipsometry, and AFM (cf. Table 1). For the −OH, −NH$_2$, and −CH$_3$ terminated SAMs, the contact angles measured were within the ranges reported previously.[10,57,58,62] For the −CH$_3$ SAM, ellipsometric film thickness was 27 Å. In previous work on −CH$_3$ terminated alkyl SAMs, the film thickness, L, was found to be given by L(Å) = 1.26n + 4.78, where n is the number of carbon atoms in the backbone.[58] Using this formula for n = 18, predicts L = 27.46 Å, essentially identical to that measured here. For the −OH terminated SAM, the thickness was consistent with the reported value of 16 Å.[58] Atomic force micrographs (see Supporting Information) indicated a very uniform monolayer for all SAM surfaces with low root-mean-square (RMS) surface roughness, and there was no evidence of large (several square nanometer) defects.

XP spectra were acquired for all four reactive surfaces examined here. The survey spectrum for chemical oxide showed three elements: silicon (2s, 153 eV; 2p, 99.7 eV),[66] oxygen (1s, 532 eV),[70] and carbon (1s, 285 eV).[58] On the chemical oxide, there is a shoulder on the high binding energy side of the Si(2p) peak (see Supporting Information) that is from the SiO$_2$ thin film. Fitting the Si(2p) feature to two peaks of equal fwhm gives a chemical shift of 3.46 eV for the peak associated with SiO$_2$, which can be compared to a value of 3.5 eV that has been previously reported[71] for chemical oxide grown using an RCA clean. Survey XP spectra for all three SAMs gave peaks only for the following components: C(1s), 285 eV; Si(2s), 153 eV; Si(2p), 99.7 eV; O(1s), 532 eV; and N(1s), 400.6−401.2 eV (only for the −NH$_2$ SAM).[62] No Cl was detected by XPS. Chemical conversion from vinyl to −OH termination was verified in two ways. First, the area of the O(1s) peak increased by 14% for the −OH SAM as compared to that observed for the underlying substrate (chemical oxide). The second observation involves the C(1s) peak (vide infra). Chemical conversion of the −CN group to −NH$_2$ was verified by examining the N(1s) peak (Figure 1) for both a −NH$_2$ terminated SAM and a −CN terminated SAM, the latter not subjected to the chemical conversion described above in section II.A. The N(1s) peak is shifted by 1.25 eV for the −NH$_2$ terminated SAM with respect to the −CN terminated SAM (0.7−1.3 eV reported previously[62]), confirming the effectiveness of the chemical conversion.

In Figure 1, we also present C(1s) spectra obtained from the −OH, −NH$_2$, and −CH$_3$ terminated SAMs. These spectra provide additional evidence as to the effectiveness of the chemical conversion and can be used to estimate the coverage of the SAMs. As may be seen, the peak for the 18-carbon chain SAM is the largest, which is expected if the 2-D packing densities are similar for the three SAMs. The spectra are best described by fits to one peak for the −CH$_3$ terminated SAM and to two peaks for the −OH and −NH$_2$ terminated SAMs. The high energy shoulders are of course associated with the terminal −CH$_2$− groups bound to the −OH and −NH$_2$ end groups. The fits give chemical shifts of 3.44 eV (cf. 1.6 eV[58]) for the −OH SAM and 2.84 eV for the −NH$_2$ SAM. In these fits, the ratios of the peak height of the chemically shifted component to that of the −CH$_2$− backbone were not free parameters but were fixed to be 0.146 for the −OH SAM and 0.137 for the −NH$_2$ SAM (calculated using $\lambda_{SAM,C(1s)}$ = 24.5 Å[72]).

As indicated above, the C(1s) feature can be used to estimate the absolute coverage of the SAMs. To accomplish this, one needs to account for the photoelectron cross-sections, σ, for the C(1s) and the Au(4f$_{7/2}$) peaks, the analyzer transmission, $T(E)$,

(69) Calistri-Yeh, M.; Kramer, E. J.; Sharma, R.; Zhao, W.; Rafailovich, M. H.; Sokolov, J.; Brock, J. D. *Langmuir* **1996**, *12*, 2747−2755.

(70) *Atomic, Molecular and Solid State Structure Studied by Means of Electron Spectroscopy*; Siegbahn, K., Nordling, C., Fahlman, A., Nordberg, A., Hamrin, K., Hedman, J., Johansson, G., Bergmark, T., Karlsson, S., Lingbren, I.; Almquist and Wiksells: Uppsala, Sweden, 1967.

(71) Wong, C. Y.; Klepner, S. P. *Appl. Phys. Lett.* **1986**, *48*, 1229−1230.

(72) Lamont, C. L. A.; Wilkes, J. *Langmuir* **1999**, *15*, 2037−2042.

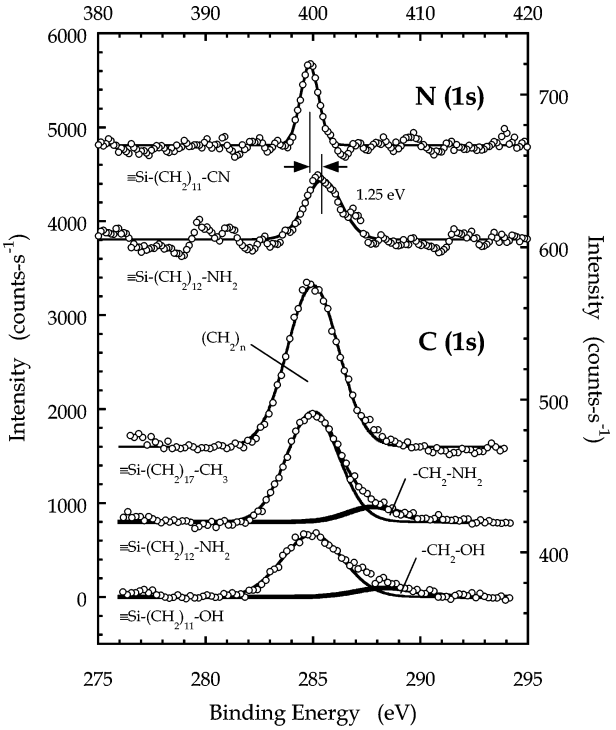

Figure 1. XP spectra of the N(1s) (upper) and C(1s) (lower) features for the SAMs considered here. The upper set of N(1s) spectra, fit to single Gaussian−Lorentzian product functions, demonstrates the chemical conversion from a −CN to a $-NH_2$ terminated SAM. The lower C(1s) spectra, fit to one ($-CH_3$ terminated SAM) or two ($-NH_2$ and −OH terminated SAMs) Gaussian−Lorentzian product functions, indicate the presence of a reactive functional group for the latter two spectra. These C(1s) spectra are also used to compute the coverage of the SAMs.

which is inversely proportional to the kinetic energy for the spectra acquired in Figure 1 (E = 968.6 and 1169.6 eV, respectively), the atomic density of the two elements, N, and the inelastic mean free path, λ, for the photoelectrons. Concerning these, $\sigma_{Au}/\sigma_C = 9.8$ [66], $N_{Au} = 5.88 \times 10^{22}$ atoms/cm^3,[73] and $\lambda_{Au} = 15.5$ Å.[74] The atomic density of C in the SAM depends on the coverage or density of the SAM, n_{SAM} (molecules/cm^2), and the mean spacing between C in the backbone, d_C. The integrated intensity of the Au($4f_{7/2}$) peak is proportional to $\sigma_{Au}N_{Au}\lambda_{Au}T(E_{Au})$. For the C(1s) peak, we must account for the finite thickness of the layer, and the integrated intensity is proportional to $\sigma_C(n_{SAM}/d_C)\lambda_C T(E_C)$ [1 − exp($-nd_C/\lambda_C \cos\theta$)], where n is the number of carbons in the SAM backbone and θ is the takeoff angle. For the inelastic mean free path of the C(1s) photoelectrons, we use $\lambda_C = 24.5$ Å.[72] Making use of these expressions and the spectra shown in Figure 1, we have computed the density of the SAMs, n_{SAM} (Table 1). Given the assumptions made here to calculate these values, we estimate that their absolute accuracy is approximately ±30%, whereas the relative accuracy should be much better, that is, ±10%. The densities range from 2.96 to 4.38 to 3.09−3.99 × 10^{14} molecules/cm^2 for the −OH, $-NH_2$, and $-CH_3$ SAMs, respectively. These values can be compared to previous work where values of 4−5, 3.7−4.2, and 5.7 × 10^{14} molecules/cm^2 have been reported for ≡Si−$(CH_2)_{17}$−CH_3 and ≡Si−$(CH_2)_{11}$−CH_3 SAMs on native oxide,[75] ═Si(CH_3)−$(CH_2)_3$−NH_2 on native oxide,[76] and ≡Si−$(CH_2)_3$−NH_2 on Davisil silica,[77] respectively.

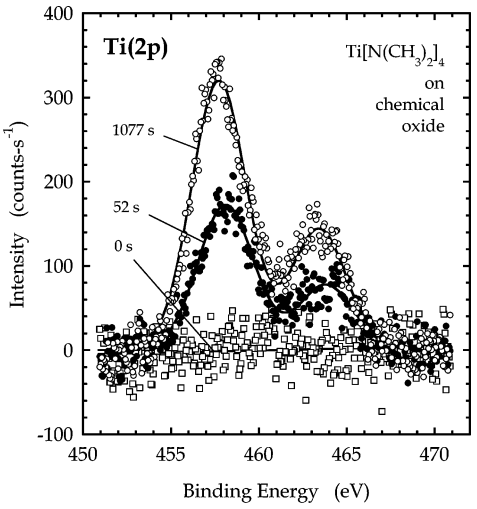

Figure 2. XP spectra of the Ti(2p) feature for a chemical oxide surface exposed to Ti$[N(CH_3)_2]_4$ at 30 °C. Spectra have been fit to two peaks using Gaussian−Lorentzian product functions. Exposure times of the surface to Ti$[N(CH_3)_2]_4$ are as indicated.

B. Reaction of Ti$[N(CH_3)_2]_4$ with the SAMs: Adsorption Kinetics. The adsorption of Ti$[N(CH_3)_2]_4$ on chemical oxide and the three SAMs possessing different end groups described above has been examined at three substrate temperatures, T_s = −50, 30, and 110 °C. In Figure 2, we plot Ti(2p) spectra for Ti$[N(CH_3)_2]_4$ adsorption on chemical oxide at T_s = 30 °C. The smooth curves represent a fit of the spectra to a mixed Gaussian−Lorentzian function where a ratio of 0.45:1 is assumed for the area of the $2p_{1/2}$ and $2p_{3/2}$ peaks.[78] As may be seen, the peak areas increase with increasing exposure. There also is a slight shift in the peak position with increasing exposure; the Ti($2p_{3/2}$) peak shifts from 458.1 (52 s) to 457.7 eV (1077 s). This shift of 0.4 eV could represent more Ti−O bonds present at low coverages, for example, $[(CH_3)_2N]_2$-Ti(−O−Si)$_2$ versus $[(CH_3)_2N]_3$Ti(−O−Si) species at high coverage.

Plotted in Figure 3 are the coverage−exposure relationships for Ti$[N(CH_3)_2]_4$ adsorption on chemical oxide, the −OH SAM, the $-NH_2$ SAM, and the $-CH_3$ SAM, all at T_s = 30 °C. A similar set of data has been collected for T_s = −50 and 110 °C (see Supporting Information). To quantify the Ti density on the surface, we collected spectra from bulk single-crystal TiO_2 (Commercial Crystal Laboratories Inc., Naples, FL) where the integrated intensity is proportional to $\sigma_{Ti}N_{Ti}\lambda_{Ti}T(E_{Ti})$ (λ_{Ti} = 20.67 Å[79] and $N_{Ti} = 3.2 \times 10^{22}$ atoms/cm^3). The titanium atoms in the Ti$[N(CH_3)_2]_4$ adlayer were modeled as a thin film of thickness d_{Ti} and titanium atomic density N'_{Ti}, whose integrated intensity is proportional to $\sigma_{Ti}N'_{Ti}d_{Ti}T(E_{Ti})/\cos\theta$, assuming $d_{Ti} \ll \lambda_{Ti}$. The quantity plotted in Figure 3 is $N'_{Ti}d_{Ti}$ (atoms/cm^2), and the greatest uncertainty in these absolute values is associated with the assumed value for λ_{Ti} (probably at least ±30%). In all cases, a number of models were fit to the data, including a first-order Langmuir model and models assuming that an extrinsic

(73) *Solid State Physics*; Ashcroft, N. W., Mermin, N. D., Eds.; Harcourt Brace College Publishers: New York, 1976.
(74) Powell, C. J.; Jablonski, A. *J. Vac. Sci. Technol. A* **1999**, *17*, 1122−1126.
(75) Wasserman, S. R.; Whitesides, G. M.; Tidswell, I. M.; Ocko, B. M.; Pershan, P. S.; Axe, J. D. *J. Am. Chem. Soc.* **1989**, *111*, 5852−5861.
(76) Moon, J. H.; Shin, J. W.; Kim, S. Y.; Park, J. W. *Langmuir* **1996**, *12*, 4621−4624.
(77) Kallury, K. M. R.; Macdonald, P. M.; Thompson, M. *Langmuir* **1994**, *10*, 492−499.
(78) Lee, H.; Lee, S. M.; Ada, E. T.; Kim, B.; Weiss, M.; Perry, S. S.; Rabalais, J. W. *Nucl. Instrum. Met. Phys. Res. B* **1989**, *157*, 226−232.
(79) Seah, M. P.; Dench, W. A. *Surf. Interface Anal.* **1979**, *1*, 2−11.

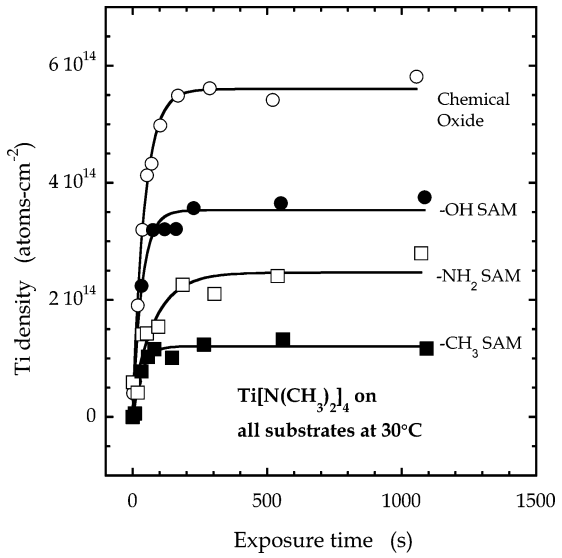

Figure 3. Coverage−exposure relationship, deduced from XPS, for the adsorption of $Ti[N(CH_3)_2]_4$ on chemical oxide and $-OH$, $-NH_2$, and $-CH_3$ terminated SAMs, at a substrate temperature of 30 °C. The fits to the data, shown as smooth curves, are for a first-order Langmuirian model of adsorption.

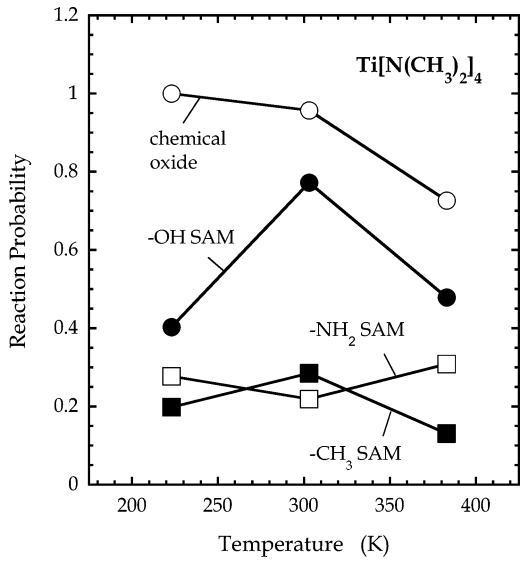

Figure 4. Initial probability of adsorption for $Ti[N(CH_3)_2]_4$ on chemical oxide and $-OH$, $-NH_2$, and $-CH_3$ terminated SAMs, as a function of substrate temperature. The data have been normalized to that observed for $Ti[N(CH_3)_2]_4$ on chemical oxide at $T_s = -50$ °C.

mobile precursor exists for adsorption (e.g., the Kisliuk model[80]). We found that the data were sufficiently well described by first-order Langmuirian kinetics, viz., $d\theta/dt = (S_{R,0}F/n_s)(1 - \theta)$, where θ is the coverage of adsorbed $Ti[N(CH_3)_2]_4$, $S_{R,0}$ is the initial probability of adsorption, F is the incident flux of $Ti[N(CH_3)_2]_4$ (molecules/cm^2/s), and n_s is the saturation coverage (molecules/cm^2).

From the fits to the data displayed in Figure 3 (and others for $T_s = -50$ and 110 °C), coupled with an estimate of the incident flux of $Ti[N(CH_3)_2]_4$, we can evaluate both the initial reaction probability, $S_{R,0}$, and the saturation coverage, n_s. In Figure 4, we plot the initial reaction probability as a function of temperature for the four surfaces examined here, where the

(80) Kisliuk, P. *J. Phys. Chem. Solids* **1957**, *3*, 95−101.

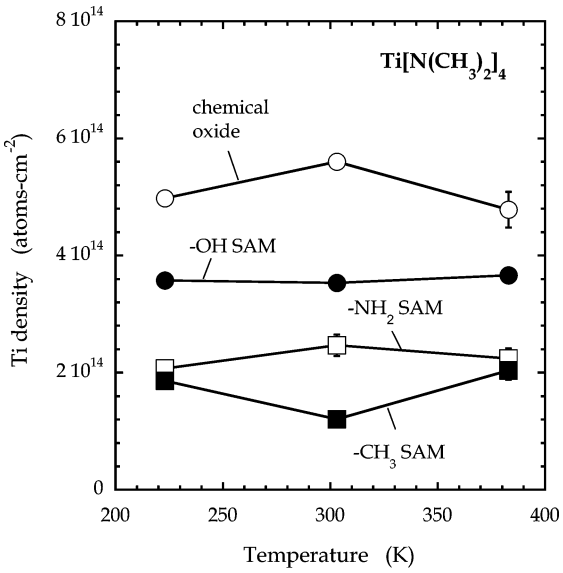

Figure 5. Concentration of titanium at saturation from the adsorption of $Ti[N(CH_3)_2]_4$ on chemical oxide and $-OH$, $-NH_2$, and $-CH_3$ terminated SAMs, as a function of substrate temperature. Densities in all cases were deduced from XPS and assumed no attenuation of the Ti(2p) photoelectrons emanating from Ti in the adlayer.

data have been normalized to the value for $S_{R,0}$ measured on chemical oxide at $T_s = -50$ °C. As may be seen, the initial reaction probability is highest on the chemical oxide, and $S_{R,0}$ decreases slightly with increasing substrate temperature. Making use of our estimate for the absolute flux of $Ti[N(CH_3)_2]_4$, we estimate that $S_{R,0} \sim 0.48$ on chemical oxide at $T_s = -50$ °C, exhibiting an average value of ∼0.43 for the reaction conditions examined here. Given the uncertainty in the values for estimates of the absolute flux and coverage, these absolute values for $S_{R,0}$ possess uncertainties of ∼50%. Next in reactivity is the $-OH$ terminated SAM, with an average value that is ∼62% of that observed on chemical oxide. Reactivities of the $-NH_2$ and $-CH_3$ terminated SAMs are comparable (30 and 23% of that on chemical oxide), and no significant trend with substrate temperature is observed. For these reaction conditions, the observation of finite reactivity with the $-CH_3$ terminated SAM is unexpected, and we consider this further below.

In Figure 5, we plot the Ti saturation coverage for the four surfaces examined here as a function of substrate temperature. This quantity exhibits only a weak dependence on substrate temperature for all four surfaces examined. In comparing the surfaces, the ranking essentially follows that observed for the initial reaction probability. The average saturation density on the chemical oxide is $\sim 5.12 \times 10^{14}$ atoms/cm^2 for the SAMs; it is 3.59, 2.26, and 1.70×10^{14} atoms/cm^2 for the $-OH$, $-NH_2$, and $-CH_3$ terminations, respectively. These values, certainly the latter, should be compared to the number density of functional groups present on the surface. In addition, these values assume there is no attenuation of the Ti(2p) photoelectrons in the adlayer.

C. Reaction of $Ti[N(CH_3)_2]_4$ with the SAMs: Microstructure of the Adlayer. The results presented above demand a more in depth analysis of the chemisorbed layer. In particular, we have found that the starting surface to the formation of the SAMs, that is, the chemical oxide, is the most reactive surface examined here. Thus, the possibility exists that the buried SAM/SiO_2 interface may retain substantial reactivity that must be

accounted for in the analysis of these results. ARXPS is a very useful technique to probe the spatial extent of reaction of Ti-$[N(CH_3)_2]_4$ with the SAMs. By varying the takeoff angle of emitted photoelectrons, those emitted by Ti atoms reacting at the SAM/SiO_2 interface are attenuated, as compared to those from the Ti atoms reacting at the top of the SAM. Consequently, the Ti peak area may decrease with increasing takeoff angle if all Ti atoms were at the SAM/SiO_2 interface, while the Ti peak area may actually increase with increasing takeoff angle if Ti atoms react with the terminal group of the SAM, owing to geometric effects.

First, we consider ARXPS of the unreacted $-CH_3$ terminated SAM, namely, the integrated areas for the O(1s) and C(1s) peaks as a function of takeoff angle (see Supporting Information). We will analyze photoemission from the SAM with a model that assumes that the underlying chemical oxide of thickness, d_{ox}, is covered uniformly by the SAM of thickness d_{SAM}. The corresponding inelastic mean free paths of the photoelectrons in the two layers are given by λ_{ox} and λ_{SAM}. The expressions used to fit the data for both emission from the C in the SAM and the O in the chemical oxide are given elsewhere (see Supporting Information). In a fit to the data, up to five parameters could be included: the intensities corresponding to the semi-infinite thin films ($I_{0,i}$) and the three attenuation factors, $(d/\lambda)_{SAM,C(1s)}$, $(d/\lambda)_{SAM,O(1s)}$, and $(d/\lambda)_{ox,O(1s)}$. To reduce the number of parameters to three, we assumed $\lambda_{SAM,C(1s)}/\lambda_{SAM,O(1s)} = \{E[C(1s)]/E[O(1s)]\}^{1/2}$ [79] and $(d/\lambda)_{ox,O(1s)} = 0.323$ from an earlier analysis of the Si(2p) spectrum for chemical oxide. From a fit to the data, we obtained $(d/\lambda)_{SAM,C(1s)} = 0.85$ and $(d/\lambda)_{SAM,O(1s)} = 0.99$. Making use of the ellipsometric thickness measured here, $d_{SAM} = 27$ Å, we find that $\lambda_{SAM,C(1s)} = 31.8$ Å, $\lambda_{SAM,O(1s)} = 27.4$ Å. These results are perhaps most useful to estimate $\lambda_{SAM,Ti(2p)} = 28.8$ Å based on $\lambda \propto E^{1/2}$.

Next, to determine the spatial extent of reaction of Ti-$[N(CH_3)_2]_4$ with the self-assembled monolayers, ARXPS was conducted on the four surfaces examined here, where in all cases, the adsorbed layer was representative of that achieved at a saturation exposure at $T_s = 110$ °C. Takeoff angles, from the surface normal, were varied from 0 to 65°. In Figure 6, we plot the integrated Ti(2p) area for saturated adlayers of Ti$[N(CH_3)_2]_4$ on the chemical oxide, $-OH$, $-NH_2$, and $-CH_3$ terminated SAMs as a function of takeoff angle. Several qualitative observations can be made at this point. First, the Ti(2p) intensity for both the chemical oxide and the $-NH_2$ terminated SAM increases with increasing takeoff angle, approximately by a factor of 2 as the angle increases from 0 to 65°. In contrast, for the $-OH$ terminated SAM, the increase is much more modest, while for the $-CH_3$ terminated SAM, a *decrease* is observed. Even in the absence of a detailed fit to the data, which we consider next, *these results indicate that there is something fundamentally different concerning the reaction of* Ti$[N(CH_3)_2]_4$ *on the* $-CH_3$ *terminated SAM, namely, significant penetration of the molecule to the underlying SAM/*SiO_2 *interface*.

To analyze the results presented in Figure 6, we are required to make assumptions as to the distribution of Ti$[N(CH_3)_2]_4$ in the near surface region. In addition, we take note of the relatively limited data set, five takeoff angles in each case. In comparison, in reference to the data collected on the bare $-CH_3$ terminated SAM, we used a three-parameter model coupled with independent information as to the thickness of the SAM and the SiO_2

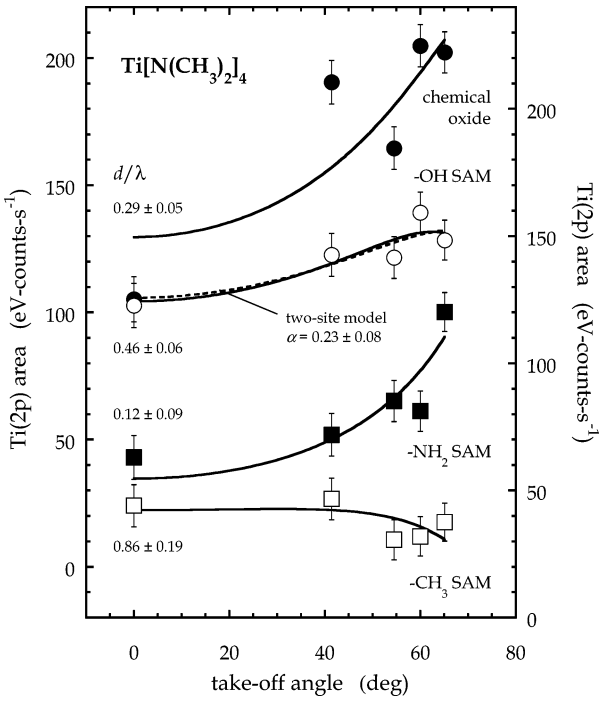

Figure 6. Peak area of the Ti(2p) region for Ti$[N(CH_3)_2]_4$ adsorbed on chemical oxide and the $-OH$ terminated SAM (left axis) and the $-NH_2$ and $-CH_3$ terminated SAMs (right axis) as a function of takeoff angle. The smooth curves are a fit to the model described in the text, which assumes that the Ti is uniformly distributed at a depth d from the surface, and the inelastic mean free path of the Ti(2p) photoelectrons is λ. The values for the parameter d/λ are shown in each case. Also shown as a dashed curve is a fit of the data for the $-OH$ SAM to a two-site model as described in the text.

layer to fit two sets of seven data points. The fit to the data in this case, which was excellent, revealed parameters with small standard errors (a few percent). Thus, we are led to make use of the simplest model that can still lead to significant conclusions. We will assume that the Ti in the adlayer is arranged in a 2-D plane at a distance (d) from the surface. This will actually be an excellent representation for the chemisorbed layer for the two limiting cases where (i) reaction is solely with the terminal organic functional end group of the SAM, and (ii) reaction is solely at the SAM/SiO_2 interface. A fit to the data involves two parameters, I_0 and d/λ, where λ is the inelastic mean free path of the Ti(2p) photoelectrons (see Supporting Information). These fits are given by the smooth curves shown in Figure 6 along with values obtained for the parameter d/λ. The parameter d/λ increases in the order: $-NH_2 \sim$ chemical oxide $< -OH < -CH_3$ SAM. The value observed for the $-NH_2$ SAM, that is, $d/\lambda = 0.12 \pm 0.09$, is consistent with the reaction of Ti-$[N(CH_3)_2]_4$ solely with the terminal $-NH_2$ group. The results for the chemical oxide, $d/\lambda = 0.29 \pm 0.05$, are also consistent with Ti$[N(CH_3)_2]_4$ being located on the surface, and a finite value may reflect both the finite thickness of the adsorbed layer [the $N(CH_3)_2$ ligands may attenuate photoemission] and the surface roughness. The results for the $-OH$ SAM are intermediate in character, $d/\lambda = 0.46 \pm 0.06$, and suggest that some penetration of the SAM may occur in this case. If we use the values for $\lambda_{SAM,Ti(2p)}$ deduced above, this suggests $d \sim 13.3 \pm 1.7$ Å, which is comparable to the thickness of the $-OH$ SAM, which is 17 Å. Finally, for the $-CH_3$ SAM, $d/\lambda = 0.86 \pm 0.19$ or $d \sim 24.8 \pm 5.5$ Å, indicating significant penetration of this SAM (thickness ~27 Å) and reaction at the SAM/SiO_2 interface.

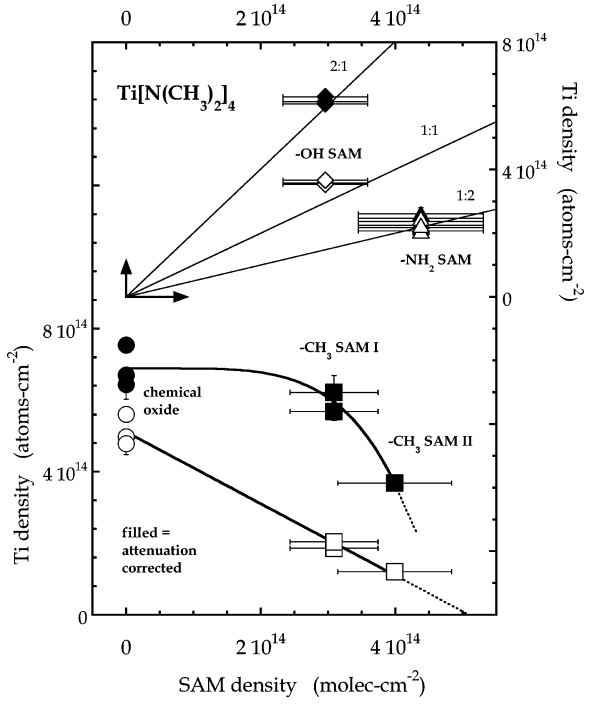

Figure 7. Relationship between the concentration of Ti in the saturated adlayers and the concentration of the molecules in the self-assembled monolayer. In the upper panel, data are displayed for the $-OH$ and $-NH_2$ terminated SAMs, in the lower, the chemical oxide and the $-CH_3$ terminated SAM. The open symbols represent the case where we have assumed that the photoemission from the Ti in the adlayer is unattenuated; the filled symbols assume that the Ti is uniformly distributed at a depth d from the surface, and the amount of attenuation has been accounted for by using the results from ARXPS (Figure 6). SAM I and SAM II refer to different batches of the $-CH_3$ terminated SAM.

As indicated above, this was the only surface that indicated a clear decrease in the Ti(2p) intensity at more glancing takeoff angles.

We can extract additional details concerning the reaction of $Ti[N(CH_3)_2]_4$ with the SAMs by examining further the results from XPS, specifically the peak positions and areas associated with the key elemental components in $Ti[N(CH_3)_2]_4$, and a comparison of the densities of the SAMs versus that for Ti in the saturated adlayers. Concerning the latter, in Figure 7, we plot the saturation density of Ti versus the SAM density, both deduced from XPS. Open symbols are the estimates for the saturation densities of Ti plotted above in Figure 5. Closed symbols are the saturation densities predicted by fits to the data that accounted for attenuation by the SAMs.

We begin the discussion with the SAM expected to be totally unreactive with $Ti[N(CH_3)_2]_4$, namely, the $-CH_3$ terminated SAM. During these experiments, we made use of one batch of $-CH_3$ SAM (marked II here) whose density was higher by ~25% than that of other SAMs examined here. Although unintentional, this allows us to examine the effect of SAM density on $Ti[N(CH_3)_2]_4$ adsorption in this case. As may be seen, there is a negative correlation between the density of Ti adsorbed and that of the $-CH_3$ SAM. This is entirely as expected in this case, as the ability of $Ti[N(CH_3)_2]_4$ to penetrate the SAM to find the reactive SAM/SiO_2 interface should increase with decreasing SAM density. These results further validate the picture of $Ti[N(CH_3)_2]_4$ adsorption on the $-CH_3$ SAM—there is no reaction with the terminal groups; it is confined completely to the SAM/SiO_2 interface. If we assume that this negative correlation between the SAM density and the Ti density is linear, a fit to both sets of estimates for the Ti density predicts that a density of $\sim 5.3 \times 10^{14}$ cm^{-2} may be sufficient to prevent penetration of $Ti[N(CH_3)_2]_4$ and reaction at the SAM/SiO_2 interface. Other assumptions, for example, including only the attenuation corrected data (but also the results on chemical oxide), lead to models where the Ti density varies in a nonlinear fashion with SAM coverage, viz., $1 - (n_{SAM}/n_{SAM,sat})^m$. A fit to this latter function gives $n_{SAM,sat} \sim (4.7 \pm 0.4) \times 10^{14}$ cm^{-2}, and $m \sim 4.8 \pm 1.9$. In either case, our results for the $-CH_3$ SAM are entirely consistent with $Ti[N(CH_3)_2]_4$ reaction at the SAM/SiO_2 interface, which might be blocked completely by a sufficiently dense SAM.

We next move to a discussion of the results for the terminal groups anticipated to be reactive. First, for the $-OH$ SAM, we see that the ratio between the density of adsorbed Ti molecules and the $-OH$ groups present on the SAM depends on the Ti estimate used; it is ~1:1 using the model that assumes Ti is present at the surface, whereas it is ~2:1 using the model that assumes all of the Ti is below the surface (~13 Å, based on the fit in Figure 6). Given this intermediate result for the $-OH$ SAM, we have made use of a more complicated, two-site model to fit the ARXPS data shown in Figure 6. Briefly, this model makes use of a weighted sum of two terms, where the Ti atoms either are present in an adlayer at the surface (at depth d_{ad}) or are buried at the SAM/SiO_2 interface (at depth d_{SAM}). We further assume that the inelastic mean free paths for the photoelectrons are identical for both layers, and we use the estimate for $\lambda_{SAM,Ti(2p)}$ calculated above. We are left with basically two parameters: I_0 and the quantity α, which we define as the fraction of Ti that is bound at the surface. Our fit to the data using this model is shown in Figure 6. We find, in this case, that $\alpha = 0.23 \pm 0.08$. In terms of absolute densities, this model predicts $(1.63 \pm 0.08) \times 10^{14}$ Ti atoms/cm^2 are bound at the terminal $-OH$ group of the SAM, whereas $(5.47 \pm 0.73) \times 10^{14}$ Ti atoms/cm^2 are at the SAM/SiO_2 interface (uncertainties do not reflect uncertainty in assumed mean free path). Concerning the former value, the Ti:SAM ratio is about 0.55, meaning each $Ti[N(CH_3)_2]_4$ molecule is bound to ~2 terminal groups, or only ~1/2 of these $-OH$ terminal groups have reacted with $Ti[N(CH_3)_2]_4$.

For the $-NH_2$ SAM, our ARXPS results are very clear. Little or no penetration has occurred, and reaction is confined to the terminal group at the surface. It should be noted that based on our results from XPS, the $-NH_2$ SAM possessed the highest density of any SAM we examined here. This is one explanation for why penetration of this SAM and reaction at the interface were not observed. Given the certainty of the location of the reaction, we are afforded the opportunity to consider the stoichiometry of the reaction in this case. As may be seen from Figure 7, our results are most consistent with a stoichiometry of Ti:SAM of between 1:2 and 2:3. The interpretation of the results can be made directly, either $\sim 1/2 - 2/3$ of the $-NH_2$ have reacted with $Ti[N(CH_3)_2]_4$ (e.g., $(R_2N)_3Ti-NH-CH_2-$..., with $1/2$ remaining unreacted), or on average, ~1.5−2 $-NH_2$ groups have reacted with each $Ti[N(CH_3)_2]_4$ [e.g., $(R_2N)_2Ti-(NH-CH_2-...)_2$]. At this point, either of the possibilities is plausible. The highest density of Ti observed on the $-NH_2$ SAM is $(2.47 \pm 0.19) \times 10^{14}$ atoms/cm^2. If this density represents a

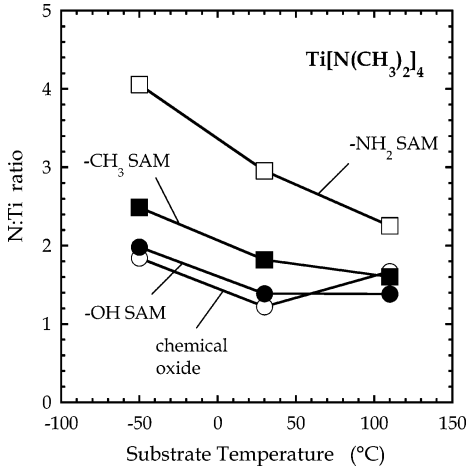

Figure 8. Ratio of N to Ti in the saturated adlayer, as deduced from XPS, for $Ti[N(CH_3)_2]_4$ adsorbed on chemical oxide and the $-OH$, $-NH_2$, and $-CH_3$ terminated SAMs as a function of substrate temperature.

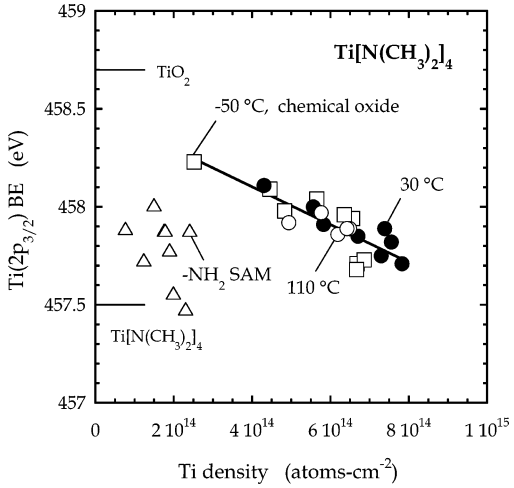

Figure 9. Binding energy of the $Ti(2p_{3/2})$ peak in the saturated adlayer [referenced to C(1s) binding energy for the same adlayer] for $Ti[N(CH_3)_2]_4$ adsorbed on chemical oxide and the $-NH_2$ terminated SAM as a function of (attenuation corrected) Ti density. Only the result for $T_s = -50$ °C for the $-NH_2$ terminated SAM is shown. Displayed also are the expected peak positions for TiO_2 and (condensed) $Ti[N(CH_3)_2]_4$.

hexagonally close-packed array of spheres, they would have a diameter of 6.8 ± 0.3 Å. This size is not unreasonable for a $Ti[N(CH_3)_2]_3(a)$ species; from the density of liquid $Ti[N(CH_3)_2]_4$, we estimate a diameter of 8 Å.

The extent of decomposition/loss of a ligand of $Ti[N(CH_3)_2]_4$ upon chemisorption can be assessed by an examination of the Ti(2p) and N(1s) peaks. First, we shall consider the ratio of the areas of these two peaks, after making suitable corrections for photoelectron cross-sections, analyzer transmission, and inelastic mean free paths. In Figure 8, we plot the N:Ti atomic ratio in the adlayer as a function of the substrate temperature following exposure to $Ti[N(CH_3)_2]_4$. For unreacted $Ti[N(CH_3)_2]_4$, this ratio is of course 4:1. Two things are apparent from the figure. First, significant decomposition [i.e., loss of the $N(CH_3)_2$ ligands] is implied by the results for $Ti[N(CH_3)_2]_4$ reacting on chemical oxide and the $-OH$ and $-NH_2$ terminated SAMs; and second, for all surfaces examined, this decomposition becomes more significant at higher temperatures (most obvious for the $-NH_2$ SAM), indicating an activated process. Chemisorption presumably involves, at minimum, loss of one $N(CH_3)_2$ ligand, thus, we expect this ratio to be either 3 or 4, depending on the identity of the linking group ($-O-$ or $-NH-$). The results for the chemical oxide, $-OH$, and $-CH_3$ SAMs seem to suggest that Ti is bound to these surfaces by 2−3 linkages, where only 1−2 $N(CH_3)_2$ ligands are retained by the parent molecule. For the $-NH_2$ SAM, based on these data alone, the situation is somewhat ambiguous, as $-NH-$ is presumably the linking group. A ratio of 4 could, in principle, be consistent with a number of scenarios. If we consider the data also shown in Figure 7, however, some of these can safely be excluded. If we take the Ti:SAM ratio to be 1:2, then an adlayer consisting of entirely $[(CH_3)_2N]_2Ti-(NH-CH_2-...)_2$ species would give a N:Ti ratio of 4. In comparison, formation of a $[(CH_3)_2N]_3Ti-(NH-CH_2-...$ species on every other $-NH_2$ SAM would give a ratio of 5. In either event, the results for the $-NH_2$ SAM also indicate considerable loss of ligand at 110 °C, where as few as one ligand may remain attached to the parent molecule ("baseline" ratio should be 2 given assumed 1:2 Ti:SAM ratio).

Examination of the chemical shift of the Ti(2p) feature can also give clues as to the nature of the species formed on the surface. Binding energy of titanium in (physisorbed) $Ti[N(CH_3)_2]_4$ has been reported to be 457.5 eV,[81] whereas that for elemental Ti and Ti bound in TiN and TiO_2 are reported to be 453.89, 455.8, and 458.7 eV, respectively.[66] We have fit the Ti(2p) feature to two peaks using Gaussian−Lorentzian product functions, identical to the procedure used above in Figure 2. In all cases, peaks were referenced to the C(1s) peak to account for effects due to the build-up of static surface charge. We will focus our discussion on the chemical oxide and the $-NH_2$ SAM. In Figure 9, we plot the Ti(2p) binding energy versus Ti density for adsorption on the chemical oxide (all temperatures) and the $-NH_2$ SAM (−50 °C only). For chemical oxide, we see essentially a linear decrease in the binding energy with increasing coverage and no strong dependence on T_s at a fixed coverage. This decrease in the binding energy is consistent with more Ti−O bonds at low coverage, whereas more bonding to N or perhaps other species (CH_x) is indicated at higher coverages. Reduced oxidation of the Ti center at high coverages could be due either to increasing steric limitations and reduced access to surface $-OH$ groups, or due to reactions of neighboring $Ti[N(CH_3)_2]_4$ fragments with each other, forming Ti−N−Ti or possibly Ti−N−C−Ti linkages. Our results for $Ti[N(CH_3)_2]_4$ reacting on the $-NH_2$ SAM are simpler to interpret and somewhat less revealing due to the scatter in the data. In brief, we see that the binding energies are all within ∼0.5 eV of that for $Ti[N(CH_3)_2]_4$ itself. Referring back to Figures 7 and 8, these results are consistent with either one or two transamination reactions with the terminal $-NH_2$ groups at $T_s = -50$ °C. That is, chemical shifts associated with replacing $N(CH_3)_2$ ligands with $NH(CH_2-CH_2-...)$ should be small.

To complete a discussion of our results, we will attempt to account for three of our most important observations: facile reaction of $Ti[N(CH_3)_2]_4$ with both surface $-OH$ and $-NH_2$ groups; a stoichiometry of Ti:$-NH_2$ SAM of ∼1:2, indicating simple ligand exchange reactions at $T_s = -50$ °C; and increased loss of ligand at elevated substrate temperatures (110 °C). Facile reaction of $Ti[N(CH_3)_2]_4$ with surface $-OH$ is of course not

(81) Corneille, J. S.; Chen, P. J.; Truong, C. M.; Oh, W. S.; Goodman, D. W. *J. Vac. Sci. Technol. A* **1995**, *13*, 1116−1120.

surprising, as it is known to react violently with water. Data concerning the reaction kinetics of Ti[N(CH$_3$)$_2$]$_4$ with −OH containing species are virtually nonexistent; however, recent calculations[82] and experiments[83] indicate that the barrier for reaction (ligand exchange) lies below the vacuum level by ∼7−14 kcal/mol. If an intrinsic precursor[84] exists to reaction of Ti[N(CH$_3$)$_2$]$_4$ on a surface with −OH groups, a barrier below the vacuum level would indicate that the reaction probability should decrease with increasing temperature. Indeed, this is observed on the chemical oxide.[83] For reaction with −NH$_2$, it is of interest to compare to predictions based on the kinetics of transamination, Ti[N(CH$_3$)$_2$]$_4$(g) + NH$_3$(g) → [(CH$_3$)$_2$N]$_3$TiNH$_2$(g) + HN(CH$_3$)$_2$(g).[47] Cross-sections for this gas-phase reaction implied by this study are predicted to increase from ∼0.44 to 4.8 × 10^{-19} cm^2 as T increases from 25 to 100 °C. Using n_{SAM} of 4.38 × 10^{14} cm^{-2} and assuming a direct gas−surface reaction implies a reaction probability of 0.19−2.1 × 10^{-4} over this same temperature range, much smaller than that observed here ($S_{R,0}$ ∼ 0.14, absolute). We also do not observe a significant dependence on temperature, whereas the gas-phase transamination reaction with NH$_3$ indicates a barrier of ∼8 kcal/mol (predicts an increase in rate of ∼2000 from T = −50 to 110 °C). The biggest difference between the gas-phase reaction and reaction on a surface involves the density of −NH$_2$ groups—reaction on a surface is more akin to a condensed-phase reaction. Recent calculations[82] have shown that the barrier for transamination can be reduced significantly (∼10 kcal/mol) in the presence of a second attacking amido ligand. Our experimental results are in agreement with this scenario, where reaction on a sufficiently dense −NH$_2$ terminated SAM is facile and essentially unactivated.

Of equal importance is the stoichiometry of the reaction with the end groups and the nature of the adlayer formed at higher temperatures, where increased loss of ligand is observed. The Ti:SAM ratio of ∼1:2 established for reaction on the −NH$_2$ SAM, and less convincingly on the −OH SAM, is consistent with the loss of two ligands at −50 °C, with the complex making two new bonds with the terminal groups of the SAMs. Assuming hexagonal close-packing, the −NH$_2$ SAMs are spaced by ∼5.1 Å, and a Ti[N(CH$_3$)$_2$]$_2$ fragment should be able to bridge these sites easily, particularly given the flexibility of the SAM alkyl backbone. Thus, at T_s = −50 °C, formation of a [(CH$_3$)$_2$N]$_2$-Ti−(NH−CH$_2$−...)$_2$ species is consistent with our data and is perhaps the best interpretation. At elevated temperatures, loss of ligand is more extensive, but it is unclear as to the nature of these reactions. Work by previous investigators may shed some light on this situation. Unimolecular decomposition of Ti[N(CH$_3$)$_2$]$_4$(g) has been the focus of a number of investigations.[43,49−51] The onset of decomposition has been reported to be at 177 [43], 205 [50], and 207 °C,[51] all of which are significantly higher than T_s ≤ 110 °C considered here. Evidence for the formation of decomposition products, such as metallacycles and imines, has been found at these elevated temperatures; formation of these species could lead to loss of ligand with no additional terminal groups involved in the reaction if these rates are sufficiently fast at T_s = 110 °C on a surface, which has not been seen previously.[43,50,51]

In our case, metallacycle formation could lead to "carbidic" (Ti−C) as opposed to "organic" carbon (alkyl and methyl carbon). For example, at much higher temperatures (350−450 °C), Fix, Gordon, and Hoffman[39] observed both organic and carbidic carbon in TiN thin films using ex situ XPS. Vepřek and co-workers[48] have also observed evidence for two, possibly three, types of carbon in this case from in situ XPS following low-pressure exposure of a Si(100) substrate to Ti[N(CH$_3$)$_2$]$_4$. We have made attempts to fit our C(1s) XP spectra for the −OH, −NH$_2$, and −CH$_3$ terminated SAMs, after saturation exposures to Ti[N(CH$_3$)$_2$]$_4$ at T_s = 110 °C, to two peaks: one at 285 eV (organic) and one at either 282 (carbidic) or 283 eV (metallacycle, assigned by Vepřek and co-workers[48]). These attempts were unsuccessful; the low binding energy peaks were essentially zero (see Supporting Information). Goodman and coworkers have speculated that loss of H from a −CH$_3$ could eliminate an N(CH$_3$)$_2$ ligand [forming HN(CH$_3$)$_2$], leaving an N(CH$_3$)═CH$_2$ ligand.[45] In our case, if a [(CH$_3$)$_2$N]$_2$Ti−(NH−CH$_2$−...)$_2$ species were present, only one ligand could be removed in this fashion. Elimination of both dimethylamido ligands by H transfer from the two SAM−NH− linkages, however, could lead to an imido complex (...CH$_2$CH$_2$N)═Ti═(N−CH$_2$−CH$_2$−...) and complete removal of the N(CH$_3$)$_2$ ligands. Indeed, in comparing saturation coverages on the −NH$_2$ SAM, we find that there is ∼20% reduction in the C(1s) peak for an increase in T_s from −50 to 110 °C, and the area for the C(1s) peak at 110 °C is ∼10% less than that of the bare −NH$_2$ SAM [both consistent with considerable loss of N(CH$_3$)$_2$ ligand]. This scenario remains an intriguing possibility, which would require additional experiments and/or theoretical calculations to verify. It is of interest to note that the bridging −O− lacks such a H to eliminate the N(CH$_3$)$_2$ ligands, consistent with the apparent retention of 1−2 ligands on surfaces with −OH present.

IV. Conclusions

The reactions of Ti[N(CH$_3$)$_2$]$_4$ with self-assembled monolayers possessing −OH, −NH$_2$, and −CH$_3$ terminal groups have been examined in detail. The initial probability of reaction of Ti[N(CH$_3$)$_2$]$_4$ was found to be largest on the chemical oxide surface (starting surface to form the SAMs), and we estimate $S_{R,0}$ ∼ 0.5 at T_s = −50 °C. On the SAM terminated surfaces, we found that reaction probabilities followed the order: −OH > −NH$_2$ > −CH$_3$. In all cases, the reaction probability did not vary more than a factor of 2 over the substrate temperature range examined, T_s = −50 to 110 °C. In addition, in all cases, the kinetics of adsorption, that is, the coverage−exposure relationships, could be sufficiently well described by a first-order Langmuirian model, and the saturation coverages did not depend strongly on the substrate temperature. Angle-resolved XPS revealed that penetration of the SAMs occurred in the cases of the −OH and −CH$_3$ terminated SAMs. In particular, the apparent reactivity between Ti[N(CH$_3$)$_2$]$_4$ and the −CH$_3$ SAM could be completely accounted for by assuming that reaction occurred only at the SAM/SiO$_2$ interface. In contrast, concerning the −NH$_2$ terminated SAM, we found that our results from ARXPS were completely consistent with Ti[N(CH$_3$)$_2$]$_4$ reaction only at the terminal −NH$_2$ group. Results for the −OH SAM indicated Ti[N(CH$_3$)$_2$]$_4$ reactivity at the terminal −OH group

(82) Haran, M.; Clancy, P. Personal communication.
(83) Ma, P. F.; Dube, A.; Killampalli, A. S.; Engstrom, J. R. In preparation.
(84) Weinberg, W. H. In *Dynamics of Gas−Surface Interactions*; Rettner, C. T., Ashfold, M. N. R., Eds; The Royal Society of Chemistry: Cambridge, 1991.

and at the SAM/SiO_2 interface. Examination of the stoichiometry of the adlayers (i.e., the Ti:N ratio) indicated that reaction of $Ti[N(CH_3)_2]_4$ and subsequent loss of ligands were significant on all surfaces, particularly for $T_s \geq 30$ °C. On all surfaces and at −50 °C, elimination of ∼2 $N(CH_3)_2$ ligands was apparent. As substrate temperature increased from −50 to 110 °C, about one additional ligand was lost on all surfaces, except for the $-NH_2$ SAM, where about 2 additional ligands were lost. On the $-NH_2$ SAM, saturation corresponded to one adsorbed $Ti[N(CH_3)_2]_4$ molecule per two SAM molecules, which is consistent with the steric limitation between $Ti[N(CH_3)_2]_4$ fragments expected for nearest neighbor distances of about 7−8 Å.

Acknowledgment. This research was supported by the Nanoscale Interdisciplinary Research Team on Inorganic−Organic Interfaces (NSF-ECS-0210693). Additional support was provided by the Cornell Center for Materials Research (CCMR), a Materials Research Science and Engineering Center of the National Science Foundation (DMR-0079992), and the Semiconductor Research Corporation via the Center for Advanced Interconnect Systems Technologies (SRC task 995.011). We also wish to thank Prof. C. T. Campbell for providing the TiO_2 single-crystal reference sample.

Supporting Information Available: Details concerning chemical oxide preparation, SAM deposition, formation of desired terminal groups, thermal stability of SAMs, delivery of $Ti[N(CH_3)_2]_4$, and estimation of $Ti[N(CH_3)_2]_4$ flux at the sample surface, XPS scan parameters. Expressions used to model data for the integrated areas of C(1s) and O(1s) peaks for the $-CH_3$ SAM and O in chemical oxide as a function of takeoff angle. Expression used to model photoemission from Ti in a 2-D adlayer at a finite depth from the surface of the SAM. This material is available free of charge via the Internet at http://pubs.acs.org.

JA047922C